Large-Scale Control of the Arabian Sea Monsoon Inversion in August

Chi-Hua Wu[1], S.-Y. Simon Wang[2,3], and Huang-Hsiung Hsu[1]

[1]Research Center for Environmental Changes, Academia Sinica, Taipei, Taiwan

[2]Utah Climate Center, Utah State University, Logan, Utah, USA

[3]Department of Plants, Soils, and Climate, Utah State University, Logan, Utah, USA

October 21, 2017

Climate Dynamics (Revised)

Corresponding author address: Chi-Hua Wu, Research Center for Environmental Changes, Academia Sinica, 128 Academia Road, Section 2, Nankang, Taipei 115, Taiwan

E-mail: chhwu@gate.sinica.edu.tw

Abstract

The summer monsoon inversion in the Arabian Sea is characterized by a large amount of low clouds and August as the peak season. Atmospheric stratification associated with the monsoon inversion has been considered a local system influenced by the advancement of the India–Pakistan monsoon. Empirical and numerical evidence from this study suggests that the Arabian Sea monsoon inversion is linked to a broader-scale monsoon evolution across the African Sahel, South Asia, and East Asia–Western North Pacific (WNP), rather than being a mere byproduct of the India–Pakistan monsoon progression. In August, the upper-tropospheric anticyclone in South Asia extends sideways corresponding with the enhanced precipitation in the subtropical WNP, equatorial Indian Ocean, and African Sahel while the middle part of this anticyclone weakens over the Arabian Sea. The increased heating in the adjacent monsoon systems creates a suppression effect on the Arabian Sea, suggesting an apparent competition among the Africa–Asia–WNP monsoon subsystems. The peak Sahel rainfall in August, together with enhanced heating in the equatorial Indian Ocean, produces a critical effect on strengthening the Arabian Sea thermal inversion. By contrast, the WNP monsoon onset which signifies the eastward expansion of the subtropical Asian monsoon heating might play a secondary or opposite role in the Arabian Sea monsoon inversion.

Keywords: African Sahel; Arabian Sea; Low Clouds; Monsoon Inversion, Western North Pacific

1. Introduction

The seasonal march of summer monsoons in South Asia, East Asia, and the WNP is characterized by a stagewise development (Murakami and Matsumoto 1994; LinHo and Wang 2002; Ding and Chan 2005; Hsu et al. 2014). Typically, the South Asian monsoon and East Asian frontal system (Meiyu–Baiu) reach a near-stationary stage in mid-June (Kato 1989; Matsumoto 1992; Sampe and Xie 2010; Tamura et al. 2010; Chou et al. 2011; Wu et al. 2017). The monsoon precipitation subsequently expands northwestward over the India–Pakistan region, setting off the Pakistan monsoon onset in mid-to-late July (Ding 2007; Wang et al. 2011). In August over the northern Arabian Sea, when the nearby monsoons have reached a mature stage, a large amount of low clouds forms in association with strong low-level atmospheric stability, creating a phenomenon called monsoon inversion (Sathiyamoorthy et al. 2013).

Atmospheric stratification (low-level thermal inversion) over the Arabian Sea has been attributed to subsidence and warm advection from the continental heat low (with a maximum intensity over West Pakistan) (Ramage 1966; Desai 1967; Narayanan and Rao 1981; Saha

2011; Dwivedi et al. 2016) and its evolution has been linked with the northward advancement of Indian summer monsoon (Bollasina and Nigam 2011; Choudhury and Krishnan 2011). The descent in the western flank of the Asia–Pacific summer monsoon may be influenced by the monsoon-desert mechanism (Rodwell and Hoskins 1996,2001); for example, an interaction between the Rossby wave in response to monsoonal heating (Matsuno 1966; Gill 1980) and the midlatitude westerly jet over the mountainous regions. The resultant subsidence from this monsoon-midlatitude interaction can cause a monsoon break in the India–Pakistan region (Ramaswamy 1962; Raman and Rao 1981; Krishnan et al. 2009; Priya et al. 2015), though its influence on the monsoon inversion has not been investigated. Moreover, the convection over the equatorial Indian Ocean, which involves the seasonal migration of the intertropical convergence zone, has a close link to the Asian summer monsoon in the north. In view of the intraseasonal northward propagations of cloud bands from the equatorial Indian Ocean onto the Indian monsoon zone, the propagations culminate further northward in the active phase of monsoon and relatively southward in the retreat phase of monsoon (Gadgil 2003; Gadgil et al. 2004).

The large-scale East Asia–WNP monsoonal circulation also undergoes transition in late July (Ueda and Yasunari 1996; Wu et al. 2009). The low-level monsoon circulation in the subtropical WNP evolves into a monsoon gyre that modulates tropical cyclogenesis (Lander 1994), while the WNP subtropical high shifts northward to the south of Japan and terminates

the Meiyu–Baiu season (Suzuki and Hoskins 2009; Ueda et al. 2009). Midlatitude perturbations were found to modulate regional monsoons, such as blocking highs that regulate the Indian monsoon break (Ramaswamy 1962; Raman and Rao 1981) and midlatitude waves affecting the East Asian–Indian summer monsoon precipitation (Krishnan and Sugi 2001; Wu 2002; Watanabe and Yamazaki 2012). Another prominent monsoon system located to the immediate west of the Arabian Sea is the West African monsoon, which matures in July and August (Quan 2003; Caley et al. 2011; Wang and Gillies 2011). However, the collective influences of the WNP monsoon, the midlatitude circulation, the Indian Ocean convection, and the West African monsoon on the Arabian Sea monsoon inversion and its peak development in August have not been explored.

In summer, the anticyclonic streamfunctions over the North Atlantic, equatorial Indian Ocean, and North Pacific surrounding the cyclonic streamfunction over South Asia characterizes the lower-tropospheric large-scale circulation (Figure 1). The changes in streamfunction from June–July to August, indicated by the color shadings in Figure 1, suggest that the major circulation components synchronously weaken. In this regard, the strengthening of Arabian Sea monsoon inversion may be affected by the seasonal transition of the surrounding large-scale circulation, instead of the development of a regional phenomenon. Little attention has been paid to the monsoonal circulation in August in relation to the Arabian Sea low clouds. We explored these associations in this study and examined

why the peak inversion in the Arabian Sea appears in August, with the perspective of a broadscale monsoon evolution. The remaining paper is organized as follows. Section 2 introduces the data and model. Section 3 details the characteristics of the Arabian Sea monsoon inversion and its evolution from June–July to August. Section 4 explores the modulation of the enhancement of the monsoon inversion through large-scale circulation. Section 5 discusses the potential mechanisms and investigation of a series of numerical experiments conducted using a simplified climate model. The concluding remarks are provided in Section 6.

2. Data and models

The observation and reanalysis data used include (a) atmospheric circulation fields obtained from the Climate Forecast System Reanalysis (CFSR) of the National Centers for Environmental Prediction (NCEP) (Saha et al. 2010) from 1979 to 2010 with a temporal resolution of 6 hourly and a 0.5° latitude-longitude spatial resolution, (b) atmospheric heating and cooling rate data during 2006–2010 retrieved from CloudSat [cloudsat.cira.colostate.edu], and (c) cloud amounts with a temporal resolution of 3 hourly during 1984–2009 obtained from the International Satellite Cloud Climatology Project (ISCCP) D1 data set (Rossow and Schiffer 1999). Although the period of CloudSat data is much shorter than the CFSR and

ISCCP, it provides vertical information of clouds in details. High-level (cloud top pressure lower than 440 hPa), middle-level (cloud top pressure lower between 440–680 hPa), and low-level (cloud top pressure higher than 680 hPa) thick clouds used in this study have an optical thickness larger than 3.6 (refer to ISCCP cloud classification). The cloud coverage (or more correctly hydrometeor cover) of ISCCP-D1 type is defined only over a large area (280 km × 280 km, i.e. 2.5°). The use of point observations to characterize the clouds is limited to making statistical assessments.

We used a simplified general circulation model (Simplified Parameterizations, privitivE-Equation Dynamics, SPEEDY), coupled with a slab ocean model to investigate the atmospheric response to a diabatic heating anomaly. The eight-layer SPEEDY model, developed by the International Centre for Theoretical Physics (ICTP), was incorporated with simplified physical parameterizations in an approximately 3.75° latitude-longitude resolution (T30) (Molteni 2003; Kucharski et al. 2005). In addition to the control simulation, we conducted seven additional simulations forced by different combination of observed 300–1000 hPa tropospheric heating difference between June 15–July 15 and August) over West Africa, the equatorial Indian Ocean, and the subtropical WNP. Input data of the SPEEDY simulation (https://www.ictp.it/research/esp/models/speedy.aspx) include climatological mean (1979–2008) soil wetness, vegetation cover, land temperature and sea-ice distribution etc. The integration length was 50 years (from 1951 to 2000) and the

outputs for the latest twenty years were analyzed.

3. The Arabian Sea monsoon inversion and low clouds

The key features of the Arabian Sea monsoon inversion consisting of temperature inversion, low-cloud formation, and the associated circulation in June–August, are shown in Figure 2. The CloudSat-retrieved heating profile over the Arabian Sea (Figure 2a, 60°E–70°E, 15°N–25°N) reveals an apparent cloud-top cooling in the lower troposphere between 800–900 hPa. The temporal evolution of low-level stability, quantified by the potential temperature difference between 1000 and 700 hPa (blue curve in Figure 2b), is closely associated with the strengthening of the warm temperature advection above 900 hPa and cold advection below; this suggests a rapid development of stabilization from mid-June to late June, followed by a continuing stabilization tendency through August and further enhanced by the low cloud-induced radiative cooling. Figure 2c outlines the appearance and dominance of low-level thick clouds in late July–early September, when the stability peaks, replacing high-level thick clouds appearing mainly in June and July (Figure 2b).

The India–Pakistan monsoon advancement likely plays a role in triggering the Arabian Sea monsoon inversion. As illustrated in Figure 2d, the strengthening of the Somali jet[1] in

[1]The strength of the Somali jet is defined as the square root of a kinetic energy of 850-hPa horizontal wind averaged over the region (50°E–70°E, 5°S–20°N), as reported by Boos WR, Emanuel KA (2009) Annual intensification of the Somali jet in a quasi-equilibrium framework: Observational composites. Quarterly

June coincides with moisture convergence at 925 hPa over the Arabian Sea (red curve in Figure 2b); this favors the development of high-level clouds associated with deep convection in 15°N–25°N (cf. Figure 2c). Low-level convergence and the Somali jet remain considerably strong in July and together, they provide a favorable atmospheric condition for the continuous development of deep convection, though the inversion acts to suppress the cloud height. The seasonal enhancement of the local Hadley circulation (Goswami et al. 1999) and thermal low (Saeed et al. 2011) in the Arabian Sea may be another factor, leading to the peak low-cloud amount in August, but this timing does not coincide with the relatively early developments of the Somali jet, Indian monsoon Hadley index, and monsoon heat low (Figure 2d).

Because the monsoon inversion mainly occurs in August, it is important to understand the circulation evolution from July to August. Figure 3 shows meridional vertical circulation over the Arabian Sea (60°E–70°E) during June 15–July 15 and in August. We use the meridional mass streamfunction Ψ_m (Oort and Yienger 1996) to represent the strength of the meridional overturning of mass. During June 15–July 15, the meridional mass-transport streamfunction indicates that the mass is transported southward and downward in the middle troposphere over the northern Arabian Sea (Figure 3a). In August, subsidence over the northern Arabian Sea is enhanced in association with the evolvement of an anticyclonic streamfunction above 500 hPa of the region (positive Ψ_m, Figure 3b). The association of the

dramatic expansion of the anticyclonic mass streamfunction in the upper troposphere and the shrinking of the cyclonic mass streamfunction in the lower troposphere is particularly strong in 15°N–30°N. The strengthened subsidence above 600 hPa associated with this vertical enhancement likely contributes to the occurrence of the Arabian Sea inversion, suggesting a remote influence from other monsoon subsystems.

4. Evolution of the large-scale circulation

This section explores the possible connection between the Arabian Sea monsoon inversion, the development of the Asian–African monsoons, and the larger-scale circulation features. In late spring and early summer, the center of the upper-tropospheric anticyclone migrates northwestward starting from the tropical western Pacific, over the Indochina Peninsula, reaches its northernmost position to the south of the Himalayas, and stays there throughout the summer (contours in Figures 4a and 4b). The development and strength of this anticyclone reflects the spring-summer evolution of the South Asian summer monsoon (Webster and Yang 1992; Sun et al. 2010). By comparing the development phase of the 200–500-hPa thickness during June 15–July 15 with that during May 15–June 15 (Figure 4a), the largest increase in the thickness is observed over East and Central Asia east of the Mediterranean Sea (Raman and Rao 1981). By August (Figure 4b), the anticyclone shifts

slightly northward in addition to noticeable zonal expansion into the WNP and the Mediterranean Sea. This zonal expansion of the upper-tropospheric anticyclone in August is accompanied by reduced zonal geopotential gradients, which potentially can influence the Arabian Sea monsoon inversion.

The latitudinal evolution of the geopotential heights at 500 hPa is further investigated in the regions (130°E–150°E, Figure 4c) and (80°E–100°E, Figure 4d). In August, the ridge of the midtropospheric high coupled with lower-tropospheric high in WNP (130°E–150°E) shifts northward to around 30°N (Figure 4c). Correspondingly, in South Asia (80°E–100°E), the meridional dipole structure in the midtropospheric geopotential height appears in August, with the highs in 25°N–35°N and the lows to the south (Figure 4d), replacing the reduced geopotential height in 10°N–30°N during June 15–July 15. The midtropospheric geopotential height increases in the subtropical India–Pakistan region in August (data not shown). In contrast to June–July, August is characterized by a high band in 25°N–35°N with relatively weak zonal asymmetry in the midtropospheric geopotential heights.

Figures 5a and 5b show the seasonal progression of the 200-hPa velocity potential from June 15–July 15 to August, in which the upper-level divergent center in South Asia and the WNP is observed. The difference between these two periods (Figure 5c) reveals an increase in upper-level convergence over the Arabian Sea, associated with the divergence and

tropospheric heating over the West Africa monsoon region, the equatorial Indian Ocean, and the WNP. From June 15–July 15 to August, the atmospheric column-integrated heating (sum of radiation, precipitation, and sensible heating) changes by 92 W m^{-2} in the subtropical WNP (SWNP; 120°E–170°E, 13°N–20.5°N), 28 W m^{-2} in the equatorial Indian Ocean (EIO; 60°E–100°E, 5°S–5°N), and 54 W m^{-2} in West Africa (WF; 20°W–30°E, 5.5°N–16.5°N).

To further illustrate the aforementioned features, we plotted the meridional cross sections of vertical circulation and mass streamfunction in Figure 6 (10°N–25°N, considering Figure 5 data). The zonal divergent wind was used for calculating the zonal mass streamfunction Ψ_z (Kamae et al. 2011). During June 15–July 15, the monsoon circulation over South and Southeast Asia is characterized by the cyclonic streamfunction (Figure 6a). By August, the ascending circulation expands eastward over 160°E and the descending circulation weakens in Africa (Figure 6b); this corresponds to the maturing of the Sahel monsoon season that spans July–September (Wang and Gillies 2011). More importantly, the relatively weak upward motion over the Arabian Sea (60°E–70°E) is further weakened (Figure 6c), suggesting a change in subsidence either induced by, or accompanied with the enhanced convection in the neighboring two larger monsoon systems. We postulate that the aforementioned development of the monsoon anticyclone and associated increases in convection in the subtropical WNP, West Africa and Equatorial Indian Ocean act to suppress the upper- to mid-level vertical motion over the Arabian Sea, leading to low clouds.

5. Numerical experiments

According to the simulation setup explained in Section 2, we investigated the atmospheric response to the diabatic heating over the SWNP, WF, and EIO regions, and their combination. As presented in Figure 5c, these regions show large heating increase from June 15–July 15 to August, i.e. 92 W m^{-2} in SWNP, 54 W m^{-2} in WF, and 28 W m^{-2} in EIO. The heating forcing given in these regions are followed as 0.92 K day^{-1} in SWNP, 0.54 K day^{-1} in WF, and 0.28 K day^{-1} in EIO, with the focus for August.

As shown in Figure 7a, the control simulation appropriately depicts the summer monsoon precipitation and circulation (in comparison with Figure 5b), although the subtropical WNP precipitation is underestimated. In the model experiments, the precipitation and circulation responses suggest that, in August, (1) the development of the subtropical WNP convection suppresses the East Asian and tropical WNP (also slightly the southern Himalayas) convection while enhancing the Bay of Bengal convection (Figure 7b); (2) heating over the equatorial Indian Ocean suppresses the convection in the Arabian Sea and Bay of Bengal (Figure 7c) while slightly enhancing the African Sahel precipitation (Figure 7d); (3) relative to individual forcing, combined effect of the WF and EIO heating on suppressing the Arabian Sea convection is the largest (Figure 7g). Critical modulation of the

EIO heating on the Arabian Sea convection is further seen (Figure 7f); (4) overall, the monsoon heating in the African Sahel together with the equatorial Indian Ocean leads to the most significant reduction in precipitation over the Arabian Sea (Figures 7e–h). While the observed development of heating in the WF, EIO, and SWNP seems to encourage subsidence in the Arabian Sea (Figure 5c), a negative effect on the Arabian Sea inversion is found when the enhanced heating is included only in the SWNP (Figure 7b). However, the SWNP's negative effect is overruled by the combined effects of WF and EIO; including the SWNP's effect makes the simulated precipitation deficit in the Arabian Sea smaller (compare Figure 7h with Figure 7g).

Figure 8 shows the simulated vertical circulation associated with diabatic heating prescribed over the SWNP, WF, and EIO regions and the results indicate the combined effects of the surrounding heating on the Arabian Sea. The zonal circulation across the Arabian Sea (10°N–25°N) indicates that enhanced heating over West Africa and the equatorial Indian Ocean heating results in an anomalous subsidence over the Arabian Sea (Figure 8b). On the contrary, the convection in the SWNP does not have a marked influence.

Figure 9 shows the large-scale circulation response in the lower troposphere associated with the prescribed heating. Combined with the heating enhancement of the equatorial Indian Ocean, the enhanced heating over West Africa induces an anomalous anticyclone over the

subtropical Southwest Asia (Figure 9c and Figure 9g). This corresponds with the weakening of the monsoon southwesterly in the lower troposphere, suppressing the monsoonal condensation and consequently the South Asian upper-level anticyclone. Notably, also combined with the heating enhancement of the equatorial Indian Ocean, the enhanced heating over the subtropical WNP strengthens the low-level westerly flow around 15°N (Figure 9b) but weakens the low-level southerly flow over India (Figure 9f). The weakening of the low-level southerly relates to the weakening of the India–Pakistan monsoon and the South Asian upper-level anticyclone. The development of African monsoon appears to produce a suppressing effect on the South Asian monsoon, while the maturing of the WNP monsoon plays a secondary or opposite role.

6. Concluding remarks

The Arabian Sea undergoes the so-called summer monsoon inversion in August associated with the formation of extensive low-level clouds. This summer monsoon inversion has been considered as a local system embedded in the India–Pakistan monsoon advancement. Unlike the mature stage of the nearby monsoons that takes place in July, the Arabian Sea monsoon inversion fully develops in August, which is concurrent with the peak monsoon precipitation in West Africa and the full development of the subtropical WNP. From July to

August, the South Asian upper-tropospheric anticyclone expands sideways over West Africa and the subtropical WNP, accompanied by the weakening of its central part over the Arabian Sea; this contributes to the enhancement of the low-level thermal inversion. Numerical experiments supported the hypothesis that the combined effects of the West Africa and subtropical WNP monsoonal heating can induce anomalous subsidence over the Arabian Sea thereby enhancing the monsoon inversion. A local Hadley circulation driven by heating in the equatorial Indian Ocean also enhances the subsidence over the Arabian Sea. In other words, the monsoon inversion and low-cloud formation in August are dynamically linked with the adjacent monsoons in West Africa and the WNP.

A schematic diagram of the aforementioned processes is presented in Figure 10. The enhanced heating in the African Sahel and the effect of the equatorial Indian Ocean, induces an anomalous anticyclone over the India–Pakistan region, weakens the South Asian upper-level anticyclone, and leads to a net reduction in the heating over the Arabian Sea. In addition, the enhanced heating over the subtropical WNP contributes to modulating the monsoon inversion through the monsoon gyre formation in August that suppresses the ascending southerlies in the Himalayan foothills and northern India–Pakistan region. The reported collective effects between the Africa–Asia–WNP monsoon subsystems on facilitating the formation of the Arabian Sea monsoon inversion in August provide a broader-scale perspective from the previously thought, namely regional processes

suppressing convection and creating low clouds.

We have also noticed that the East Asia–WNP monsoon and Arabian Sea monsoon inversion could be closely related regarding the interannual and decadal variations. Because the associated mechanisms may be more complicated than in seasonal variation, it was not focused in this study. According to the data analysis in the focused period in the current study, low clouds over the Arabian Sea were reduced in most years before the 21st century, implying a decadal variation. In years (or decades) with reduced low clouds over the Arabian Sea, the East Asian midlatitude jet stream remained strong in August, while the WNP monsoon trough weakened (not shown by the figure). Additional studies are warranted to investigate the potential modification of the synchronously seasonal changes among the monsoon subsystems in a changing climate.

Acknowledgments. This work was supported by the Consortium for Climate Change Study Phase II (CCliCS–II) under the auspices of the Ministry of Science and Technology (MOST), Taiwan, under grant MOST 105–2119–M–001–018–. CHW was also supported by MOST 105–2119–M-001–021– and 106–2111–M-001–004–. We are grateful for the model SPEEDY from the ICTP and the datasets available from the NCEP, ISCCP, and CloudSat. We also thank the three anonymous reviewers for their constructive comments.

References

Bollasina M, Nigam S (2011) The summertime "heat" low over Pakistan/northwestern India: evolution and origin. Clim Dyn 37:957-970 10.1007/s00382-010-0879-y

Boos WR, Emanuel KA (2009) Annual intensification of the Somali jet in a quasi-equilibrium framework: Observational composites. Quarterly Journal of the Royal Meteorological Society 135:319-335 10.1002/qj.388

Caley T, Malaize B, Revel M, Ducassou E, Wainer K, Ibrahim M, Shoeaib D, Migeon S, Marieu V (2011) Orbital timing of the Indian, East Asian and African boreal monsoons and the concept of a 'global monsoon'. Quaternary Science Reviews 30:3705-3715 10.1016/j.quascirev.2011.09.015

Chou MD, Wu CH, Kau WS (2011) Large-Scale Control of Summer Precipitation in Taiwan. Journal of Climate 24:5081-5093 10.1175/2011jcli4057.1

Choudhury AD, Krishnan R (2011) Dynamical Response of the South Asian Monsoon Trough to Latent Heating from Stratiform and Convective Precipitation. Journal of the Atmospheric Sciences 68:1347-1363 10.1175/2011jas3705.1

Desai BN (1967) The Summer Atmospheric Circulation over the Arabian Sea. Journal of the Atmospheric Sciences 24:216-220 10.1175/1520-0469(1967)024<0216:tsacot>2.0.co;2

Ding YH (2007) The variability of the Asian summer monsoon. Journal of the Meteorological Society of Japan 85b:21-54 DOI 10.2151/jmsj.85B.21

Ding YH, Chan JCL (2005) The East Asian summer monsoon: an overview. Meteorol Atmos Phys 89:117-142 10.1007/s00703-005-0125-z

Dwivedi S, Narayanan MS, Ratnam MV, Rao DN (2016) Characteristics of monsoon inversions over the Arabian Sea observed by satellite sounder and reanalysis data sets. Atmos Chem Phys 16:4497-4509 10.5194/acp-16-4497-2016

Gadgil S (2003) THE INDIAN MONSOON AND ITS VARIABILITY. Annual Review of Earth and Planetary Sciences 31:429-467 10.1146/annurev.earth.31.100901.141251

Gadgil S, Vinayachandran PN, Francis PA, Gadgil S (2004) Extremes of the Indian summer monsoon rainfall, ENSO and equatorial Indian Ocean oscillation. Geophysical Research Letters 31:n/a-n/a Artn L12213
10.1029/2004gl019733

Gill AE (1980) Some Simple Solutions for Heat-Induced Tropical Circulation. Quarterly Journal of the Royal Meteorological Society 106:447-462 DOI 10.1256/smsqj.44904

Goswami BN, Krishnamurthy V, Annamalai H (1999) A broad-scale circulation index for the interannual variability of the Indian summer monsoon. Quarterly Journal of the Royal Meteorological Society 125:611-633 DOI 10.1256/smsqj.55411

Hsu HH, Zhou TJ, Matsumoto J (2014) East Asian, Indochina and Western North Pacific Summer Monsoon - An update. Asia-Pacific J Atmos Sci 50:45-68 10.1007/s13143-014-0027-4

Kamae Y, Ueda H, Kitoh A (2011) Hadley and Walker Circulations in the Mid-Pliocene Warm Period Simulated by an Atmospheric General Circulation Model. Journal of the Meteorological Society of Japan 89:475-493 10.2151/jmsj.2011-505

Kato K (1989) Seasonal Transition of the Lower-Level Circulation Systems around the Baiu Front in China in 1979 and Its Relation to the Northern Summer Monsoon. Journal of the Meteorological Society of Japan 67:249-265

Krishnan R, Sugi M (2001) Baiu rainfall variability and associated monsoon teleconnections. Journal of the Meteorological Society of Japan 79:851-860 DOI 10.2151/jmsj.79.851

Krishnan R, Kumar V, Sugi M, Yoshimura J (2009) Internal Feedbacks from Monsoon–Midlatitude Interactions during Droughts in the Indian Summer Monsoon. Journal of the Atmospheric Sciences 66:553-578 10.1175/2008jas2723.1

Kucharski F, Molteni F, Bracco A (2005) Decadal interactions between the western tropical Pacific and the North Atlantic Oscillation. Clim Dyn 26:79-91 10.1007/s00382-005-0085-5

Lander MA (1994) Description of a Monsoon Gyre and Its Effects on the Tropical Cyclones in the Western North Pacific during August 1991. Weather and Forecasting 9:640-654 Doi 10.1175/1520-0434(1994)009<0640:Doamga>2.0.Co;2

LinHo, Wang B (2002) The Time–Space Structure of the Asian–Pacific Summer Monsoon: A Fast Annual Cycle View*. Journal of Climate 15:2001-2019 10.1175/1520-0442(2002)015<2001:ttssot>2.0.co;2

Matsumoto J (1992) The Seasonal-Changes in Asian and Australian Monsoon Regions. Journal of the Meteorological Society of Japan 70:257-273

Matsuno T (1966) Quasi-Geostrophic Motions in the Equatorial Area. Journal of the Meteorological Society of Japan. Ser. II 44:25-43

Molteni F (2003) Atmospheric simulations using a GCM with simplified physical parametrizations. I: model climatology and variability in multi-decadal experiments. Clim Dyn 20:175-191 10.1007/s00382-002-0268-2

Murakami T, Matsumoto J (1994) Summer Monsoon over the Asian Continent and Western North Pacific. Journal of the Meteorological Society of Japan 72:719-745

Narayanan MS, Rao BM (1981) Detection of Monsoon Inversion by Tiros-N Satellite. Nature 294:546-548 DOI 10.1038/294546a0

Oort AH, Yienger JJ (1996) Observed interannual variability in the Hadley circulation and its connection to ENSO. Journal of Climate 9:2751-2767 Doi 10.1175/1520-0442(1996)009<2751:Oivith>2.0.Co;2

Priya P, Mujumdar M, Sabin TP, Terray P, Krishnan R (2015) Impacts of Indo-Pacific Sea Surface Temperature Anomalies on the Summer Monsoon Circulation and Heavy Precipitation over Northwest India–Pakistan Region during 2010. Journal of Climate 28:3714-3730 10.1175/jcli-d-14-00595.1

Quan X (2003) Interdecadal change in the Asia–Africa summer monsoon and its associated changes in global atmospheric circulation. Global and Planetary Change 37:171-188 10.1016/s0921-8181(02)00200-x

Ramage CS (1966) The Summer Atmospheric Circulation over the Arabian Sea. Journal of the Atmospheric Sciences 23:144-150 10.1175/1520-0469(1966)023<0144:tsacot>2.0.co;2

Raman CRV, Rao YP (1981) Blocking Highs over Asia and Monsoon Droughts over India. Nature 289:271-273 DOI 10.1038/289271a0

Ramaswamy C (1962) Breaks in the Indian Summer Monsoon as a Phenomenon of Interaction between the Easterly and the Sub-Tropical Westerly Jet Streams. Tellus 14:337-349 10.1111/j.2153-3490.1962.tb01346.x

Rodwell MJ, Hoskins BJ (1996) Monsoons and the dynamics of deserts. Quarterly Journal of the Royal Meteorological Society 122:1385-1404 DOI 10.1002/qj.49712253408

−− (2001) Subtropical anticyclones and summer monsoons. Journal of Climate 14:3192-3211 Doi 10.1175/1520-0442(2001)014<3192:Saasm>2.0.Co;2

Rossow WB, Schiffer RA (1999) Advances in understanding clouds from ISCCP. Bulletin of the American Meteorological Society 80:2261-2287 Doi 10.1175/1520-0477(1999)080<2261:Aiucfi>2.0.Co;2

Saeed S, Muller WA, Hagemann S, Jacob D, Mujumdar M, Krishnan R (2011) Precipitation variability over the South Asian monsoon heat low and associated teleconnections. Geophysical Research Letters 38:n/a-n/a Artn L08702
10.1029/2011gl046984

Saha K (2011) Some aspects of the Arabian sea summer monsoon. Tellus A 26:10.3402/tellusa.v26i4.9852

Saha S, Moorthi S, Pan HL, Wu XR, Wang JD, Nadiga S, Tripp P, Kistler R, Woollen J, Behringer D, Liu HX, Stokes D, Grumbine R, Gayno G, Wang J, Hou YT, Chuang HY, Juang HMH, Sela J, Iredell M, Treadon R, Kleist D, Van Delst P, Keyser D, Derber J, Ek M, Meng J, Wei HL, Yang RQ, Lord S, Van den Dool H, Kumar A, Wang WQ, Long C, Chelliah M, Xue Y, Huang BY, Schemm JK, Ebisuzaki W, Lin R, Xie PP, Chen MY, Zhou ST, Higgins W, Zou CZ, Liu QH, Chen Y, Han Y, Cucurull L, Reynolds RW, Rutledge G, Goldberg M (2010) The Ncep Climate

Forecast System Reanalysis. Bulletin of the American Meteorological Society 91:1015-1057 10.1175/2010bams3001.1

Sampe T, Xie SP (2010) Large-Scale Dynamics of the Meiyu-Baiu Rainband: Environmental Forcing by the Westerly Jet. Journal of Climate 23:113-134 10.1175/2009jcli3128.1

Sathiyamoorthy V, Mahesh C, Gopalan K, Prakash S, Shukla BP, Mathur AK (2013) Characteristics of low clouds over the Arabian Sea. J Geophys Res-Atmos 118:13489-13503 10.1002/2013jd020553

Sun Y, Ding YH, Dai AG (2010) Changing links between South Asian summer monsoon circulation and tropospheric land-sea thermal contrasts under a warming scenario. Geophysical Research Letters 37:n/a-n/a Artn L02704
10.1029/2009gl041662

Suzuki S, Hoskins B (2009) The Large-Scale Circulation Change at the End of the Baiu Season in Japan as Seen in ERA40 Data. Journal of the Meteorological Society of Japan 87:83-99 10.2151/jmsj.87.83

Tamura T, Taniguchi K, Koike T (2010) Mechanism of upper tropospheric warming around the Tibetan Plateau at the onset phase of the Asian summer monsoon. Journal of Geophysical Research 115:n/a-n/a 10.1029/2008jd011678

Ueda H, Yasunari T (1996) Maturing process of the summer monsoon over the Western North Pacific - A coupled ocean/atmosphere system. Journal of the Meteorological Society of Japan 74:493-508

Ueda H, Ohba M, Xie S-P (2009) Important Factors for the Development of the Asian–Northwest Pacific Summer Monsoon*. Journal of Climate 22:649-669 10.1175/2008jcli2341.1

Wang S-Y, Gillies RR (2011) Observed Change in Sahel Rainfall, Circulations, African Easterly Waves, and Atlantic Hurricanes Since 1979. International Journal of Geophysics 2011:1-14 10.1155/2011/259529

Wang SY, Davies RE, Huang WR, Gillies RR (2011) Pakistan's two-stage monsoon and links with the recent climate change. J Geophys Res-Atmos 116:n/a-n/a Artn D16114
10.1029/2011jd015760

Watanabe T, Yamazaki K (2012) Influence of the Anticyclonic Anomaly in the Subtropical Jet over the Western Tibetan Plateau on the Intraseasonal Variability of the Summer Asian Monsoon in Early Summer. Journal of Climate 25:1291-1303 10.1175/Jcli-D-11-00036.1

Webster PJ, Yang S (1992) Monsoon and Enso - Selectively Interactive Systems. Quarterly Journal of the Royal Meteorological Society 118:877-926 DOI 10.1002/qj.49711850705

Wu C-H, Chou M-D, Fong Y-H (2017) Impact of the Himalayas on the Meiyu–Baiu migration. Clim Dyn 1-13 10.1007/s00382-017-3686-x

Wu CH, Kau WS, Chou MD (2009) Summer monsoon onset in the subtropical western North Pacific. Geophysical Research Letters 36:Artn L18810, 10.1029/2009gl040168

Wu RG (2002) A mid-latitude Asian circulation anomaly pattern in boreal summer and its connection with the Indian and East Asian summer monsoons. International Journal of Climatology 22:1879-1895 10.1002/joc.845

Figures

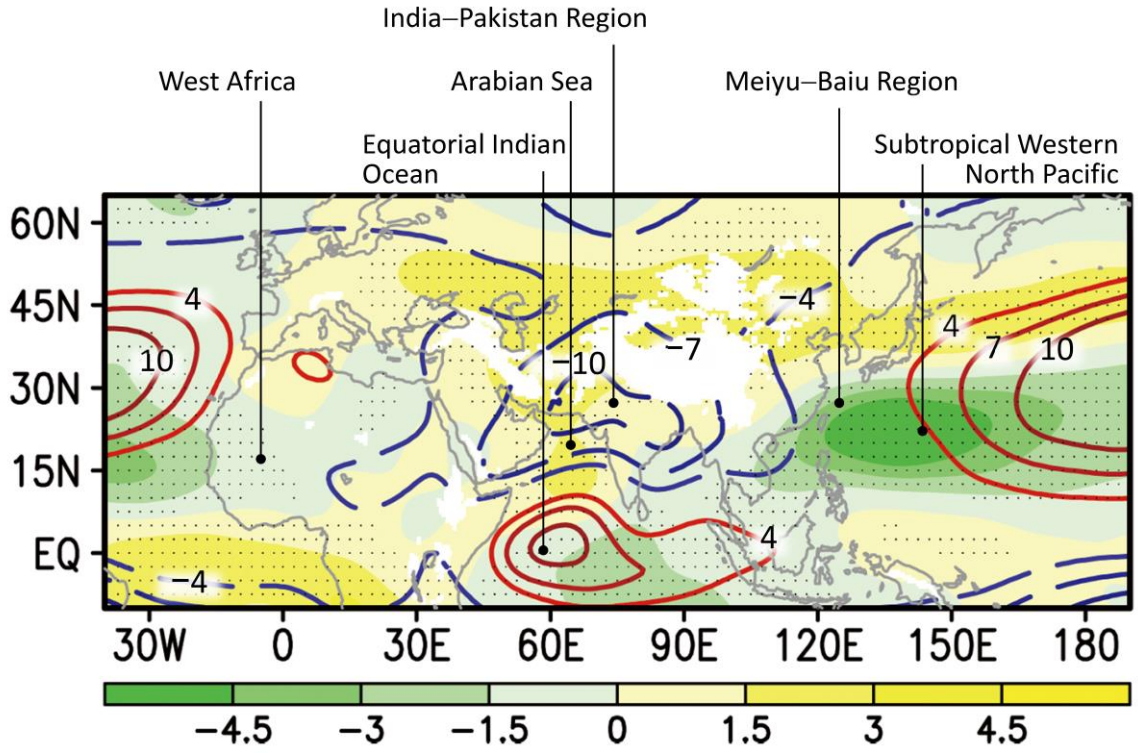

Figure 1

The 850-hPa streamfunction (contours with unit of 10^6 m^2 s^{-1}) in August and changes from June 15 to July 15 (color shadings, differences with a 95% confidence level are marked with dots).

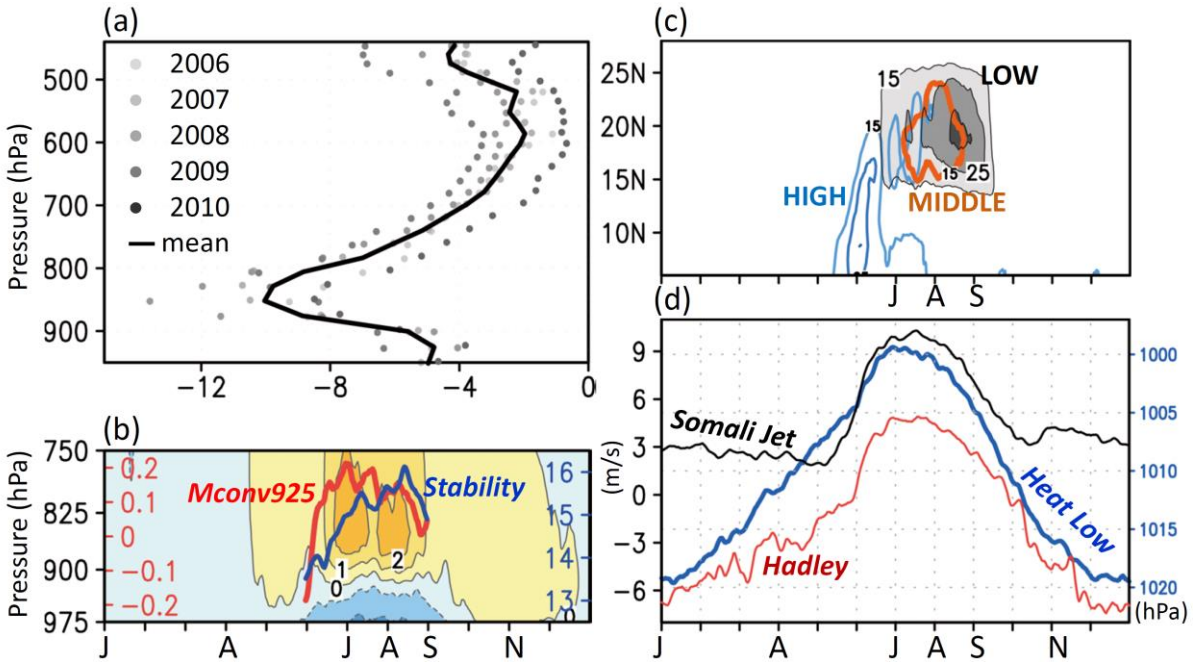

Figure 2

(a) Vertical profile of the atmospheric heating rate in August over the Arabian Sea (dots: 2006–2010; solid line: 5-year average). (b) Temporal pressure distribution of temperature advection (K day^{-1}) and JJA evolution of the 925-hPa moisture convergence (red co-ordinate and line, g kg^{-1} day^{-1}) and stability (blue co-ordinate and line, K, defined by the potential temperature difference between 700 and 1000 hPa) over the Arabian Sea (60°E–70°E, 15°N–25°N). (c) High-level (blue contours), middle-level (orange contours), and low-level (gray shadings) cloud amount (%) in the 60°E–70°E band. (d) The annual cycle of three monsoon indices: the black line denotes the strength of Somali jet stream (m s^{-1}) defined by the twice square root of kinetic energy of 850-hPa horizontal wind averaged over the region (50°E–70°E, 5°S–20°N); the red line denotes the Indian monsoon Hadley index (m s^{-1}) defined by the meridional wind shear in (70°E–110°E, 10°N–30°N) between 200 and 850 hPa; the blue line denotes the India–Pakistan monsoon heat low defined by the mean sea level pressure (hPa) in (55°E–75°E, 25°N–35°N).

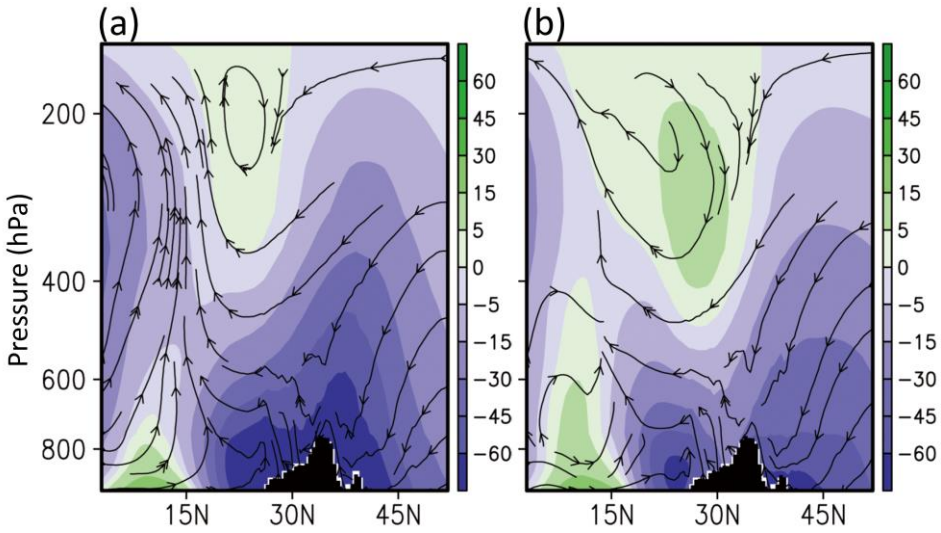

Figure 3

Meridional circulation in 60°E–70°E in (a) June 15–July 15 and (b) August. The streamlines consist of v (m s^{-1}) and omega (×100 Pa s^{-1}); color shadings denote the mass streamfunction Ψ_m (10^{10} kg s^{-1}). Black bars denote topography.

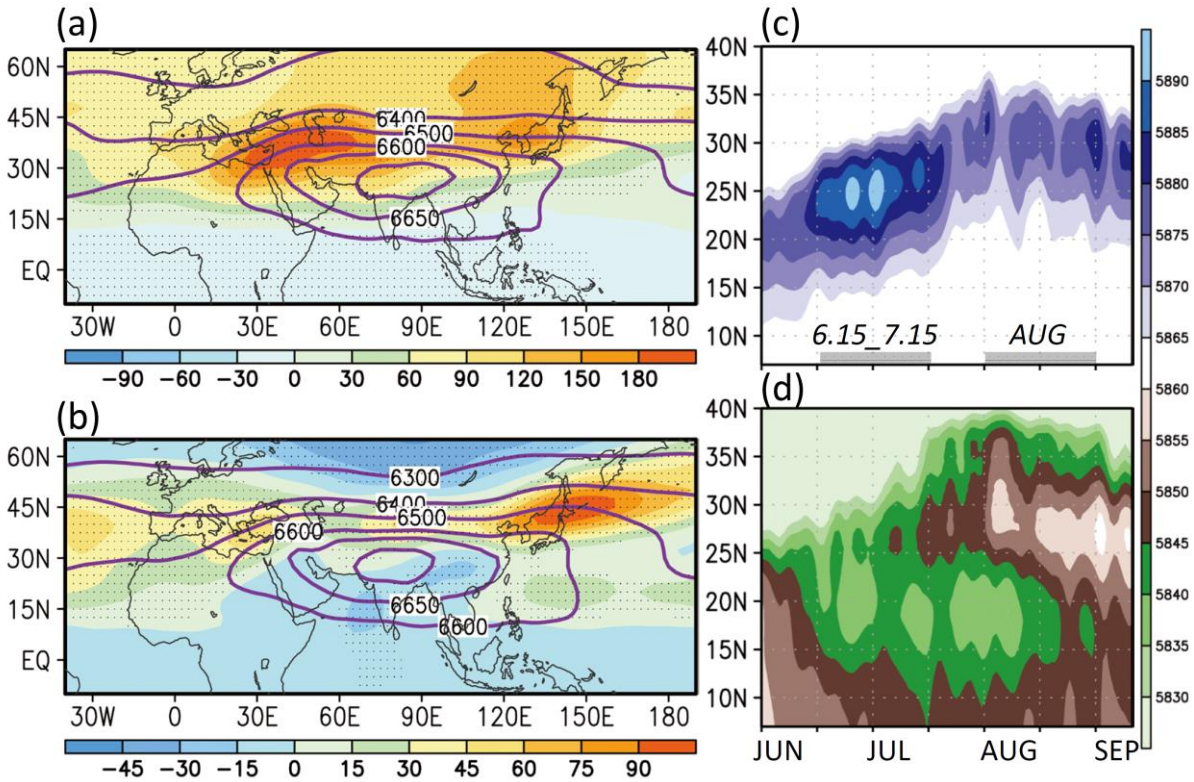

Figure 4

(a) Geopotential depth (200–500 hPa, gpm) in June 15–July 15 (contours) and changes from May 15 to June 15 (color shadings). Differences with a 95% confidence level are marked with dots. (b) Same as (a) except for August (contours) and changes from June 15–July 15 to August (shadings). (c and d) Latitude-time cross sections of the 500-hPa geopotential heights

in 130°E–150°E and 80°E–110°E.

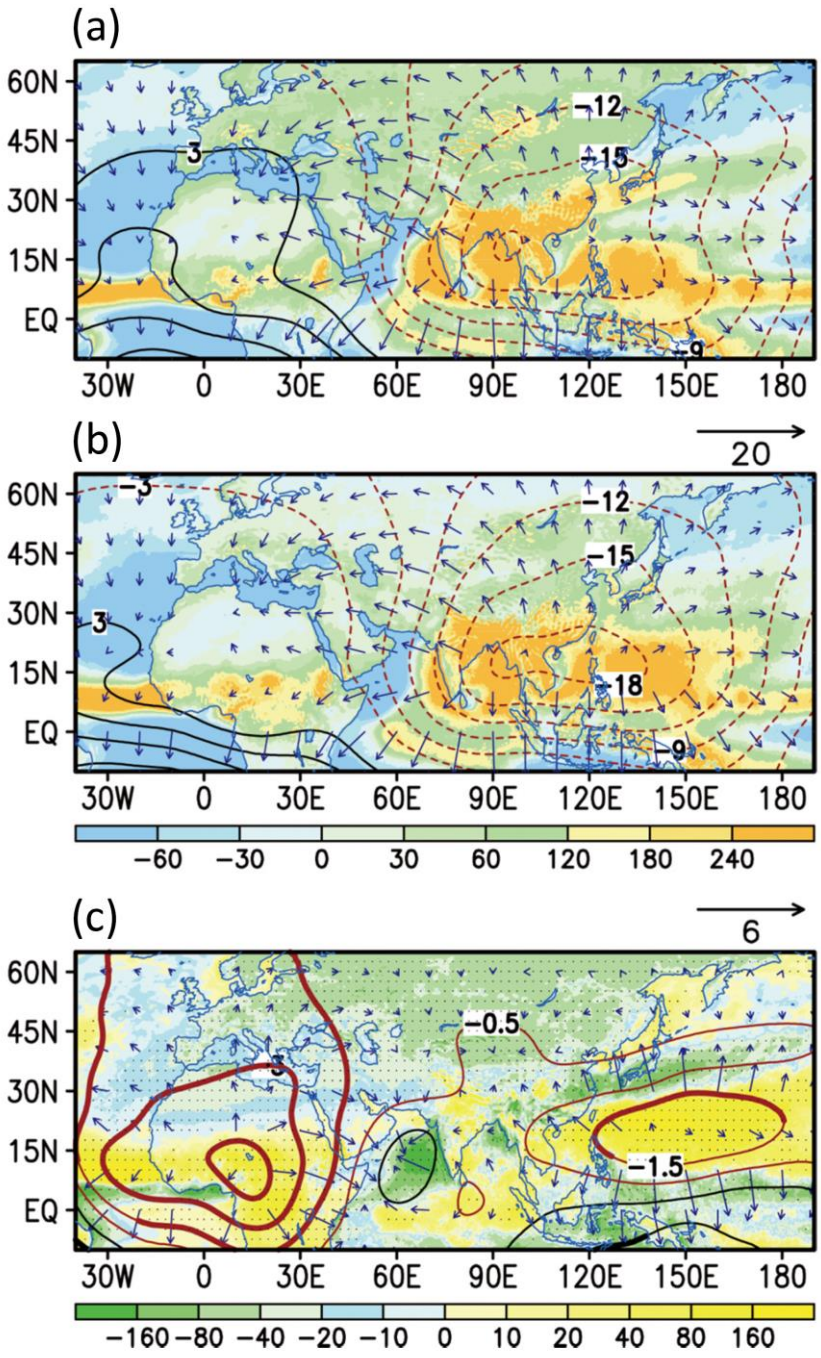

Figure 5

Atmospheric column-integrated heating (sum of radiation, precipitation, and sensible heating, shadings with unit of W m^{-2}) and the 200-hPa divergent winds (vectors, unit: m s^{-1}) and velocity potential (contours with unit of 10^6 m^2 s^{-1}) in (a) June 15–July 15, (b) August, and (c) between June 15–July 15 and August. Differences with a 95% confidence level are marked with dots or thick contour lines.

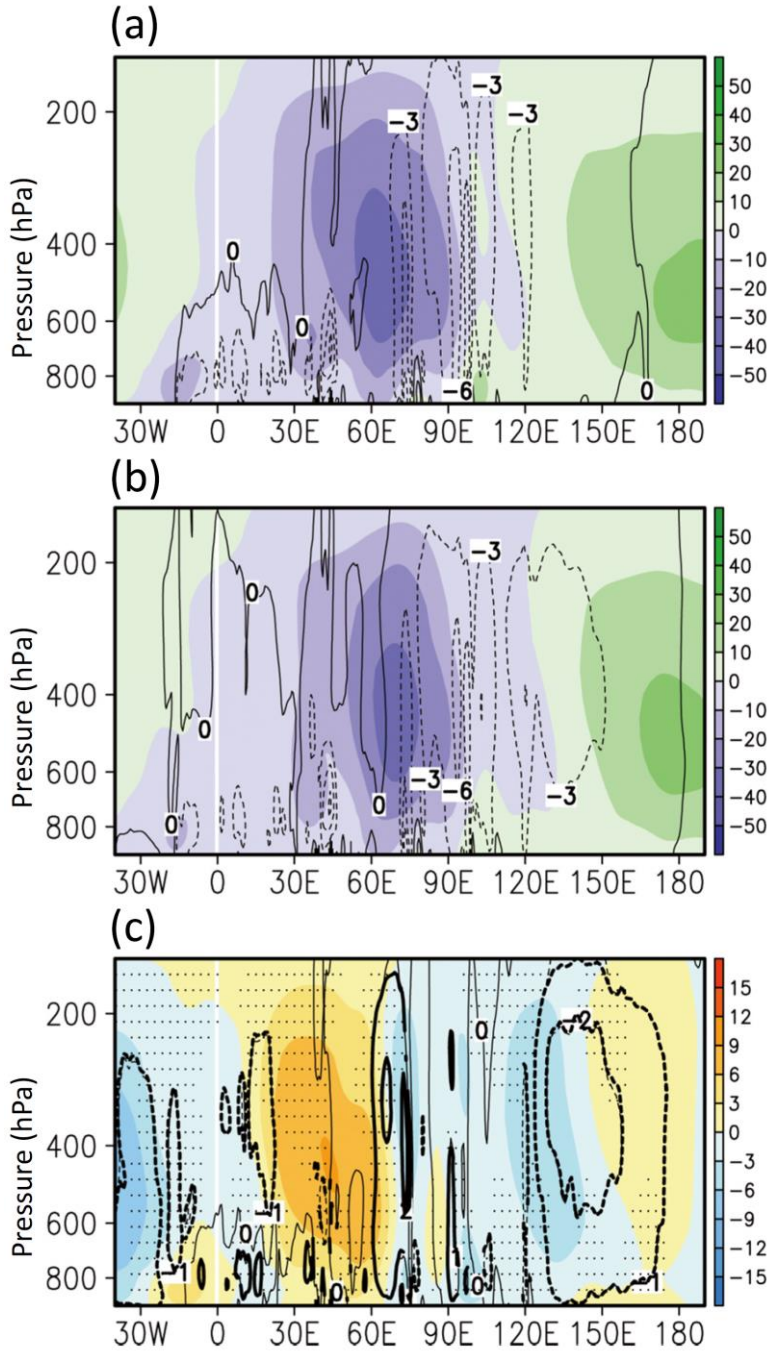

Figure 6

Zonal circulation in 10°N–25°N in (a) June 15–July 15, (b) August, and (c) between June 15–July 15 and August. Contour lines denote omega (Pa min^{-1}) and color shadings denote the mass streamfunction Ψ_z (10^{10} kg s^{-1}). Differences with a 95% confidence level are marked with dots or thick contour lines.

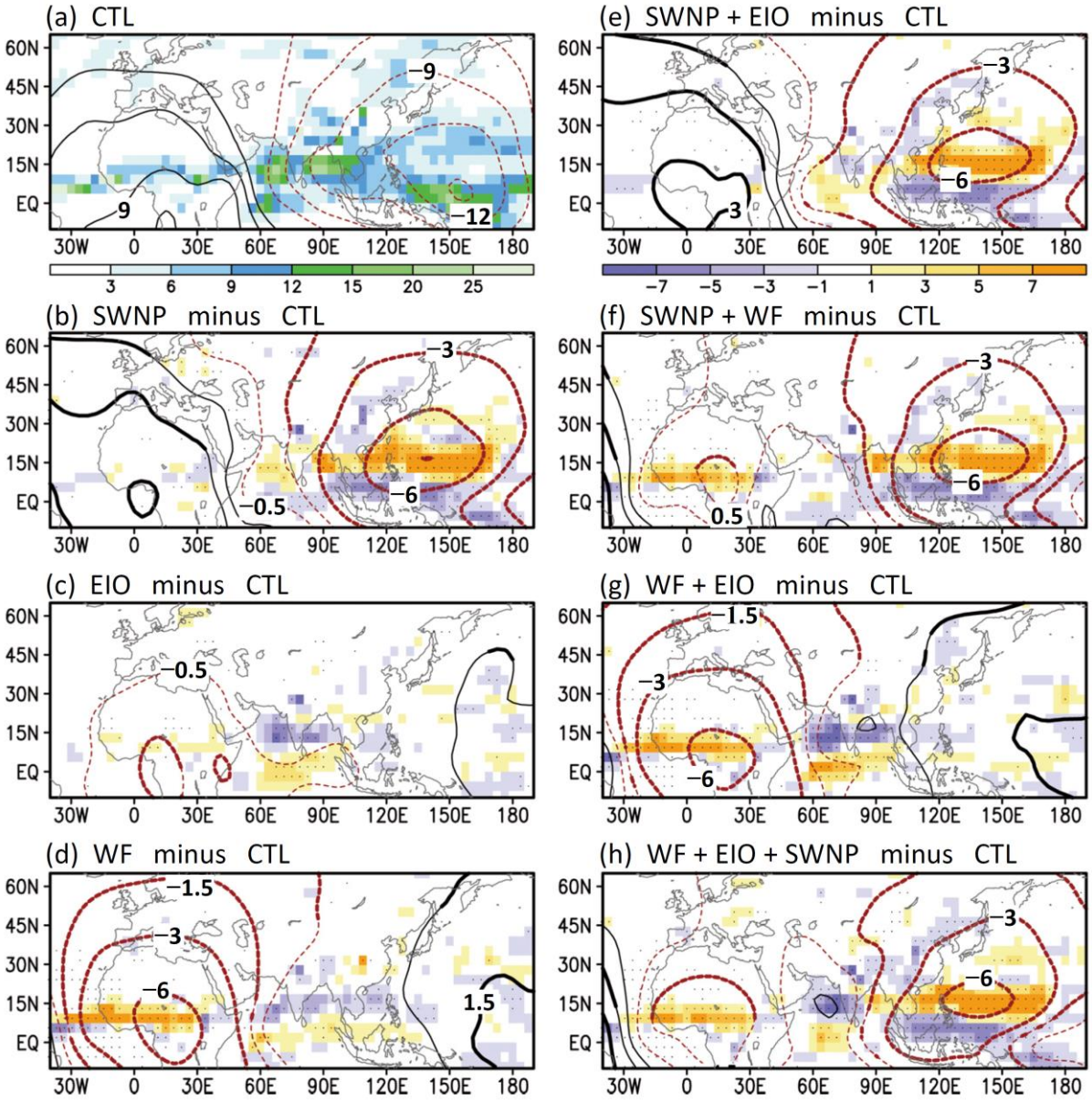

Figure 7

Precipitation (shadings, mm day^{-1}) and the 200-hPa velocity potential (contours, 10^6 m^2 s^{-1}) of the control simulation in August (a) and response to the heating forcing (b–h, minus control simulation). Fixed heating regions are (b) SWNP; (c) EIO; (d) WF; (e) SWNP+EIO; (f) SWNP+WF; (g) WF+EIO; (h) WF+EIO+SWNP. Differences with a 95% confidence level are marked with dots or thick contour lines.

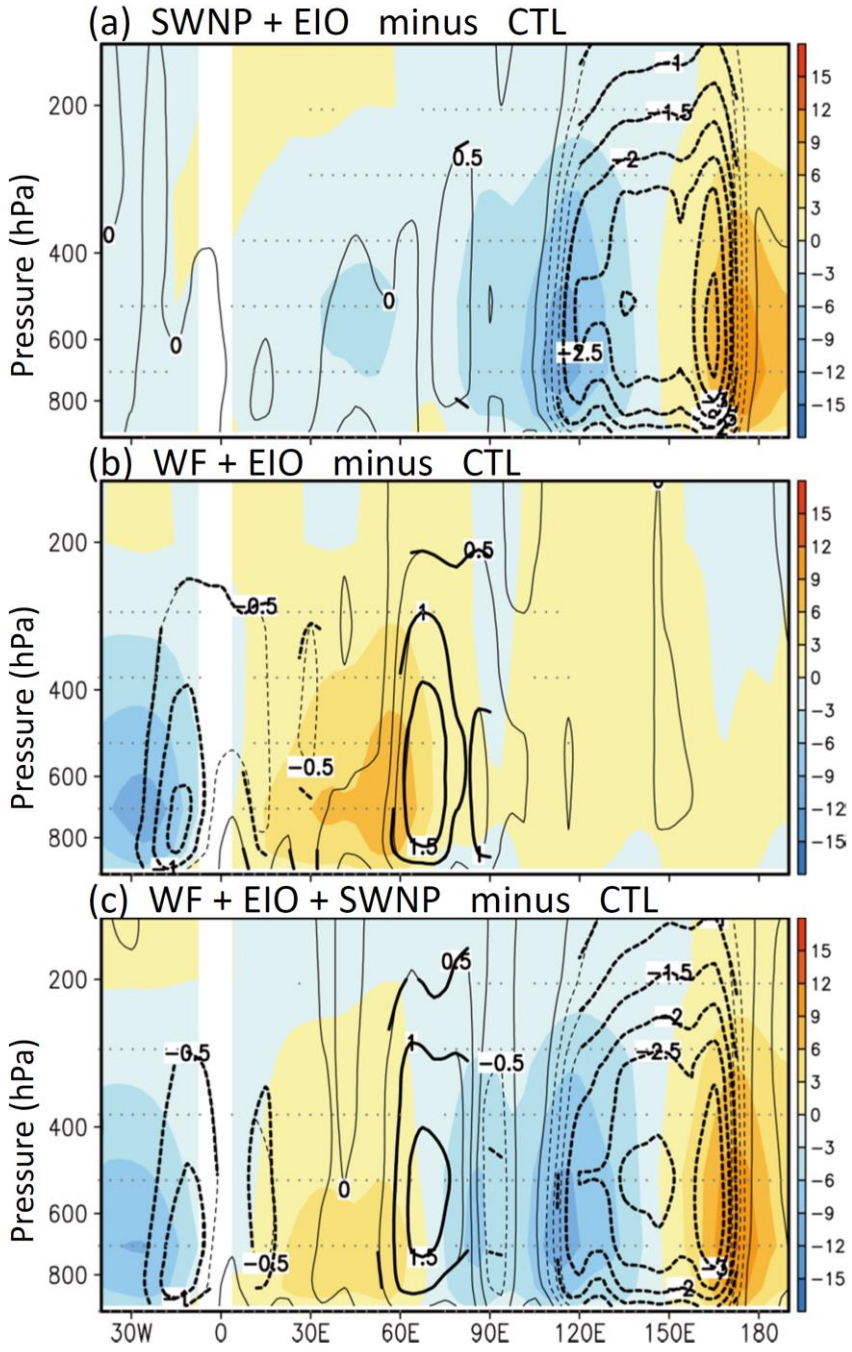

Figure 8

Zonal mass streamfunction Ψ_z (color shadings, 10^{10} kg s^{-1}) and omega (contours, Pa min^{-1}) in 10°N–25°N for responses (minus the control simulation) to (a) SWNP+EIO heating, (b) WF+EIO heating, and (c) WF+EIO+SWNP heating in August. Differences with a 95% confidence level are marked with dots or thick contour lines.

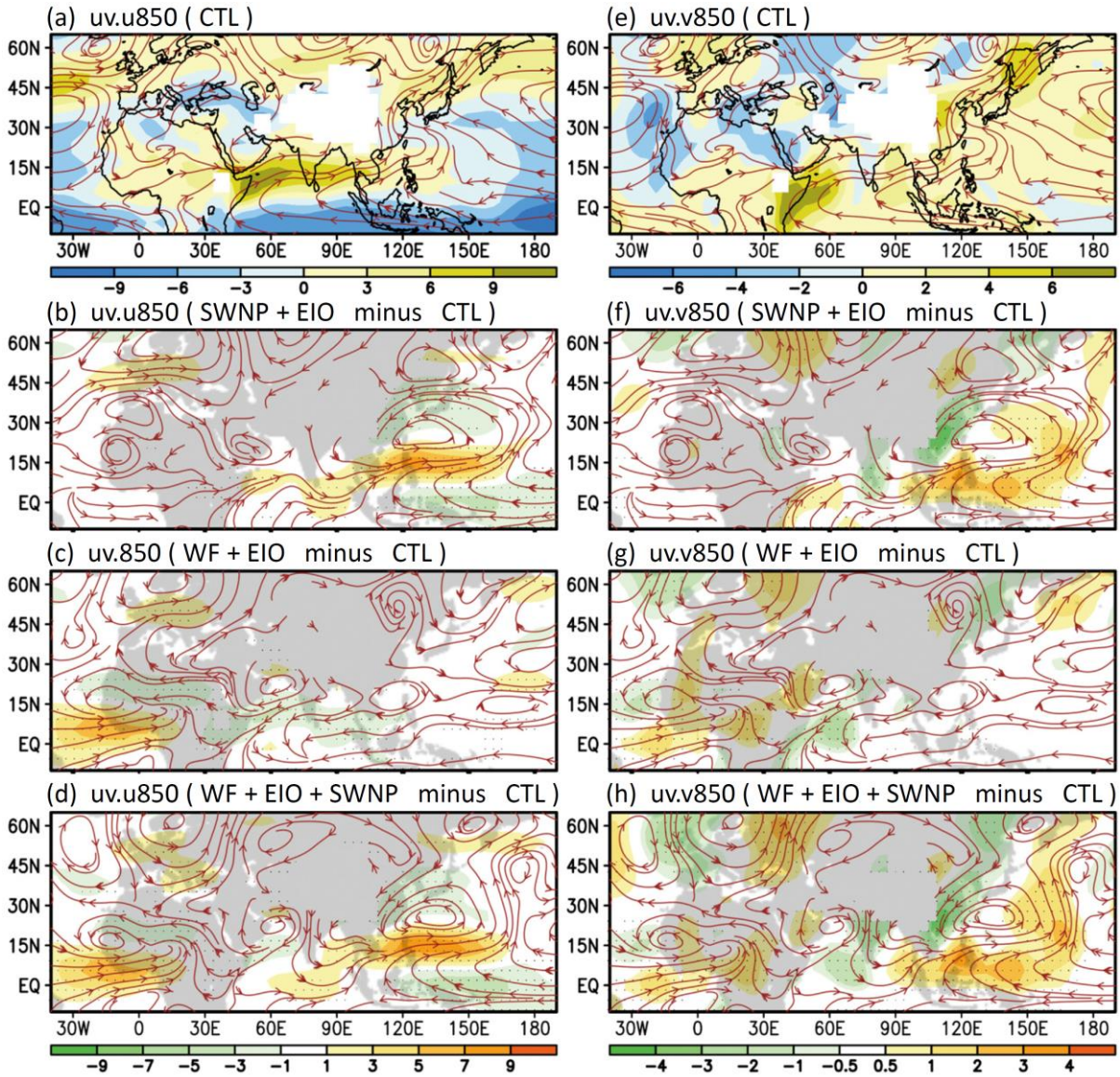

Figure 9

The 850-hPa streamlines and (a–d) zonal wind speeds and (e–h) meridional wind speeds (shadings, m s^{-1}). (a and e) the control simulation; (b and f) SWNP+EIO minus the control simulation; (c and g) WF+EIO minus the control simulation; (d and h) WF+EIO+SWNP minus the control simulation. Differences with a 95% confidence level are marked with dots.

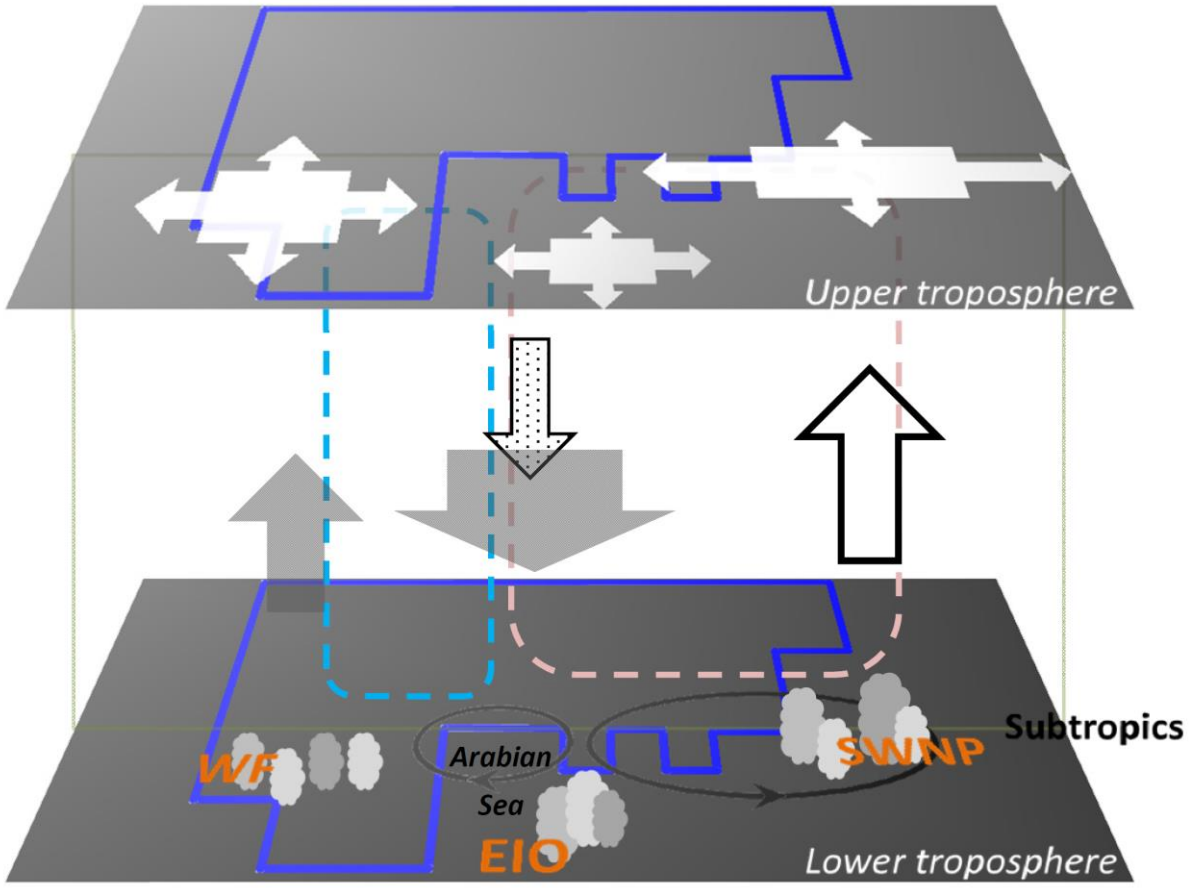

Figure 10

Schematic diagram of broadscale monsoon evolution from July to August. Combined with the heating enhancement of the equatorial Indian Ocean (EIO), peak West African (WF) monsoon rainfall induces an anomalous anticyclone in the lower troposphere of the India–Pakistan region, weakens the South Asian upper-level anticyclone, and leads to a net reduction in the heating over the Arabian Sea (gray shading arrows). The enhanced heating over the subtropical WNP (SWNP) is associated with the monsoon gyre formation, which enhances the Bay of Bengal convection whereas suppresses the ascending southerlies in the Himalayan foothills and northern India–Pakistan region. The monsoon inversion of the Arabian Sea results from the competition among the Africa–Asia–WNP monsoon subsystems, in August as the peak season.